Effect of acquisition parameters on equivalent time and equivalent bandwidth algorithms for partial discharge clustering

Rodrigo Mor, A.; Castro Heredia, L. C.; Muñoz, F. A.

DOI
10.1016/j.ijepes.2016.12.017

Publication date
2017

Document Version
Final published version

Published in
International Journal of Electrical Power & Energy Systems

Citation (APA)
Rodrigo Mor, A., Castro Heredia, L. C., & Muñoz, F. A. (2017). Effect of acquisition parameters on equivalent time and equivalent bandwidth algorithms for partial discharge clustering. *International Journal of Electrical Power & Energy Systems*, *88*, 141-149. https://doi.org/10.1016/j.ijepes.2016.12.017

Electrical Power and Energy Systems 88 (2017) 141–149

Contents lists available at ScienceDirect

Electrical Power and Energy Systems

journal homepage: www.elsevier.com/locate/ijepes

Effect of acquisition parameters on equivalent time and equivalent bandwidth algorithms for partial discharge clustering

A. Rodrigo Mor [a], L.C. Castro Heredia [a,*], F.A. Muñoz [b]

[a] Delft University of Technology, Electrical Sustainable Energy Department, Delft, The Netherlands
[b] Universidad del Valle, Escuela de Ingeniería Eléctrica y Electrónica, Cali, Colombia

ARTICLE INFO

Article history:
Received 26 August 2016
Received in revised form 16 November 2016
Accepted 26 December 2016
Available online 5 January 2017

Keywords:
Partial discharges
Clustering techniques
Phase resolved partial discharge pattern
Equivalent time
Equivalent bandwidth

ABSTRACT

The acquisition parameters of an unconventional Partial Discharge (PD) measuring system affect the way the PD pulses are recorded and in turn, the results of the data processing. The noise based on the oscilloscope's vertical resolution is a feature of the sampled signal that is always present when a digital acquisition system is used. In PD unconventional systems, several parameters such as the sampling frequency Fs, the acquisition time T, the number of samples N and the vertical resolution VR of the digitizer result in a wide oscilloscope-based noise variation, that could be quantified by the signal to noise ratio (snr).

The classification map is a tool that came available with the development of unconventional systems, that due to their wide bandwidth are able to resolve PD pulses in time and apply clustering techniques for PD source separation. The equivalent time T_{eq} and equivalent bandwidth W_{eq}, used to plot the classification map, attempts to extract features of the PD pulses to form clusters so that classification of sources can be achieved. The classification map is based on the ability of separating PD sources by resorting to the parameters T_{eq} and W_{eq}, that are believed to show significant differences for distinct PD sources, while they are clearly consistent for the same source.

This paper conducts a set of theoretical analysis and laboratory measurements to evaluate the influence of the oscilloscope-based noise on the results of T_{eq} and W_{eq}. The results proved that the classification map is heavily influenced by the signal to noise ratio.

1. Introduction

Partial discharge (PD) measurements are successfully used for diagnostics and monitoring of high voltage equipment. The technique finds a broad application scope by taking advantage of many of the physical properties that can be detected or measured from a PD event. Depending on the device under test, measurements are based on detection of acoustic emissions, chemical byproducts or current/voltage pulses in an external circuit [1]. The electrical method, i.e. the recording and processing of an electric signal induced in a detection circuit, is the most frequently used technique for detection and quantification of the PD magnitudes.

Since the PD signals occur as fast pulses having a duration of much less than the period of the power frequency waveform, specific requirements regarding the bandwidth of the measuring systems are to be met depending on the PD parameter of interest. Test and measuring circuits for apparent charge, in compliance with IEC60270 requirements, are described in [2] and are referred to as conventional systems. With such an instrument is also possible to compute phase resolved PD patters (PRPD) as a tool to assist in the recognition of PD sources. This is based on the fact that each PD source can be linked to a particular pattern (some examples of PRPD patterns are shown in [3]). If just a single source is active, the recognition process through the PRPD patterns is an easy task that can be achieved by an expert or even by an automatized system [4]. When multiples sources are active, the recognition of sources is no longer possible by resorting to a database of well-identified patterns for single sources. In these cases, a large number of unconventional test circuits have been researched. Typically, unconventional test circuits have extended the bandwidth of the measuring systems up to the MHz range or even GHz range. A bandwidth increase has the advantage of approaching the PD pulse shape. Conversely, in conventional systems the pulse phase occurrence and the pulse charge are the only two measured parameters that are acquired from each single pulse.

Unconventional systems became available with the development of modern wideband digitizers that are able to record and store thousands of individual pulses for further processing. Having the pulses resolved in time, the research efforts have been directed

* Corresponding author.
E-mail address: l.c.castroheredia@tudelft.nl (L.C. Castro Heredia).

http://dx.doi.org/10.1016/j.ijepes.2016.12.017
0142-0615/

towards what is referred to as *feature extraction*. Assumptions are made that PD pulses coming from the same source should have similar shapes. Therefore, from the clustering point of view, the objective is to find any collection of features that show significant differences for distinct PD sources, while being clearly consistent for the same source, so that clusters can be formed in a plot. This approach has come up with different techniques to separate and recognize PD sources. Ranging from [5–10] all these techniques also deal with the need of detecting and cancelling external signals (noise) coupled to the measuring circuit. In on-field testing, noise, disturbances and interferences can give rise to complex PRPD patterns or clusters, leading to misleading interpretations.

Although each technique has proven to be suitable and even when they have gained practical application, it might be still difficult to compare results from different techniques and measuring devices. This has much to do with the PD-phenomena itself. Being a PD pulse an event that cannot be measured directly, but only the response of a detection circuit, then the results from a digital PD system become strongly affected by the particular parameters of each measuring system; detection circuit plus acquisition unit.

This paper aims to research several factors affecting the equivalent time and equivalent bandwidth cluster of the PD pulses (also referred to as *classification map*), taking into account the noise based on the vertical resolution of the acquisition system. To show the influence of the acquisition parameters, the results of a theoretical analysis and lab measurements are described in the following sections.

2. Set-up description

Measurements were conducted by means of an unconventional PD system comprised of a high frequency current transformer (HFCT) type sensor having a bandwidth of 34.4 kHz–60 MHz and two acquisition units. The first one was based on a high performance oscilloscope Tektronix DPO7354C with 8 bits of vertical resolution and maximum sampling frequency of 40 GS/s. The second one was a PXI acquisition card from National Instruments with 12 bits of vertical resolution and 200 MS/s sampling rate. The measuring circuit is shown in Fig. 1.

Acquisition parameters such as sampling frequency, vertical range and sampling period were then varied depending on the requirements of the test object. The high performance oscilloscope has some desirable features like for instance a 'Fast Frame Acquisition Mode' with enhanced capabilities for pulsed signal recording. Using this feature, the trigger rearming time is normally below 1 μs, which avoids to miss much PD pulses that arrive narrowly spaced. Once a PD pulse has fired the trigger level, a number of N samples are recorded. Each recorded pulse is called a frame. The maximum number of recorded frames depends on the sampling frequency and the sampling period.

The testing program included the use of electrodes for laboratory measurements of corona discharges, surface discharges and free moving particle type discharges. Dimensions and other details related to the electrodes can be found in [11].

Data processing was achieved by means of a software tool developed by TU Delft for the purposes of the test platform reported in [11]. Both the synchronization and the PD pulse signals

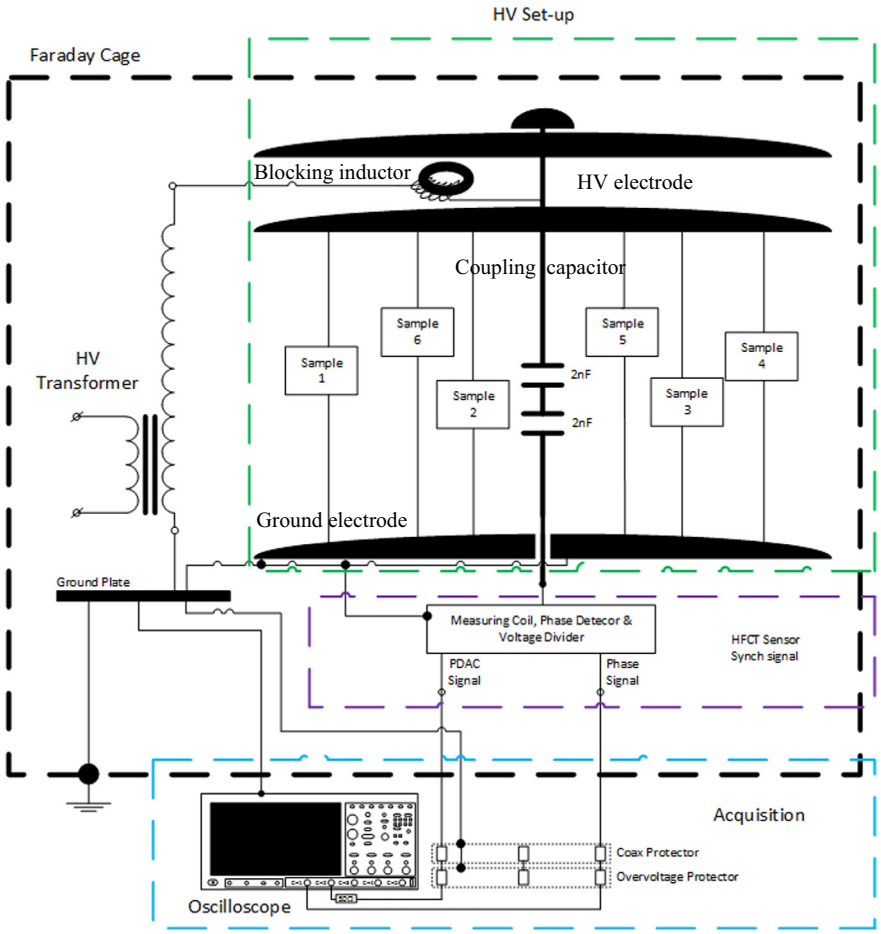

Fig. 1. Scheme of the partial discharge test platform.

were recorded by the oscilloscope. The data were processed by the software tool to estimate the charge in both frequency and time domain [12], build the PRPD patterns and apply clustering techniques.

3. PD pulse classification

The classification process of multiple PD sources mainly consists in finding a set of suitable features that show significant differences for distinct PD sources, whereas they are clearly consistent for the same source. If the selected features succeed in extracting relevant information, a cluster in a Cartesian plot is formed for each group of pulses with homogeneous characteristics. Then, each cluster can be linked to a particular PD source by resorting, e.g. to the PD-pulse height and the phase distribution analysis [13]. Thus, the classification process can be considered as a process of separation into clusters, followed by a one of recognition. In next sections, only the separation process will be discussed.

The features of a PD pulse can be any parameter directly associated with the pulse shape, such as the pulse width, the rise time, the fall time, and the peak value, or any other parameter derived from the pulse shape. Equivalent time and equivalent bandwidth are a pair of derived parameters used extensively for classification purposes (classification map). This technique has been researched over the last decades [13,14] and since then has encountered wide practical and industrial application. Currently, some standard-type technical documents related to the measurement of partial discharge on AC rotating machines [3,15] provide examples of the use of the classification map for the recognition of PD sources in stator windings.

The cluster based on equivalent time T_{eq} and equivalent bandwidth W_{eq} requires the computation of Eqs. (1)–(3) over each sampled PD pulse signal $s_i(t_i)$.

$$t_0 = \frac{\sum_{i=1}^{N} t_i s_i(t_i)^2}{\sum_{i=1}^{N} s_i(t_i)^2} \tag{1}$$

$$T_{eq}^2 = \frac{\sum_{i=1}^{N} (t_i - t_0)^2 s_i(t_i)^2}{\sum_{i=1}^{N} s_i(t_i)^2} \tag{2}$$

$$W_{eq}^2 = \frac{\sum_{i=1}^{N} f_i^2 |S_i(f_i)|^2}{\sum_{i=1}^{N} |S_i(f_i)|^2} \tag{3}$$

The time t_0 is then the mean time of the signal weighted by the power of the signal. The equivalent time T_{eq} can be understood as the second statistical moment (standard deviation) of time, where again the weighting factor is the power of the signal. The parameter W_{eq} computes the mean frequency weighted by the frequency spectrum and usually is interpreted as the equivalent bandwidth of the sampled signal $s_i(t_i)$.

Due to the widespread application of the classification map, the following sections will focused on relevant parameters that affect the results from Eqs. (1)–(3).

3.1. Factors affecting classification map

Whenever an unconventional measuring system is implemented for digital acquisition of PD signals, apart from the distortion/attenuation due to the measuring circuit and pulse propagation, the sampled signal $s_i(t_i)$ and correspondingly the signal to noise ratio (snr) is affected by the acquisition parameters such as the sampling frequency Fs, the acquisition time T, the number of samples N and the vertical resolution VR of the digitizer.

This is a consequence of the definition of snr as given by Eq. (4), where the snr entails the computation of the energy of the wanted signal v and the noise signal n.

$$snr = \frac{\sum_{i=1}^{N} v_i^2}{\sum_{i=1}^{N} n_i^2} \tag{4}$$

Eq. (4) can lead to several interpretations, e.g. the longer the acquisition time T of a short-pulse signal, the lower the snr. If the acquisition time T extends significantly compared to the pulse duration, then the value of the denominator in Eq. (4) will become predominant. A similar result comes from the increase of the magnitude of noise, i.e. an increase of n_i magnitude. In modern oscilloscopes, parameters Fs, T, N and VR can be varied in a wide range, which directly impacts on the sampling of the signal. Many academic papers and technical documents are focused on the direct application of the classification map on measured data, however they provide little or no insights regarding optimal setting of acquisition parameters.

Two scenarios were analyzed in order to test the classification map against the acquisition parameters. Firstly, artificial pulses were given different signal to noise ratios. Secondly, a number of lab measurements were conducted on distinct PD sources with varied Fs, T, N and VR. Then, the classification map algorithm from Eqs. (1)–(3) were computed on the data. The results of these analysis are discussed in the next sections.

3.1.1. Classification map for artificial pulses

For this analysis two sets of 604 artificial pulses each were generated in a math software. Pulses of type y_i and x_i have the analytical shape described by Eqs. (5) and (6) respectively.

$$y_i = t \cdot e^{-10^8 \cdot t} \tag{5}$$

$$x_i = t^{10} \cdot e^{-20^9 \cdot t} \tag{6}$$

The sampling frequency Fs was set to 200 MS/s and the acquisition time was 1200 ns. To simulate the HFCT sensor, both types of pulses were filtered by an order 2 Butterworth filter, bandpass type with 30 kHz–60 MHz cut-off frequencies. The filter output is normalized to the unity. Then, white noise was added from 20 to 60 dB range to each normalized pulse.

In Fig. 2, filtered outputs of pulses y_i and x_i are shown in the top row and bottom row respectively, scaled to 100 pC. Pulses at the left side are the noiseless pulses, and at the right side there are examples of 20 dB signal to noise ratio pulses.

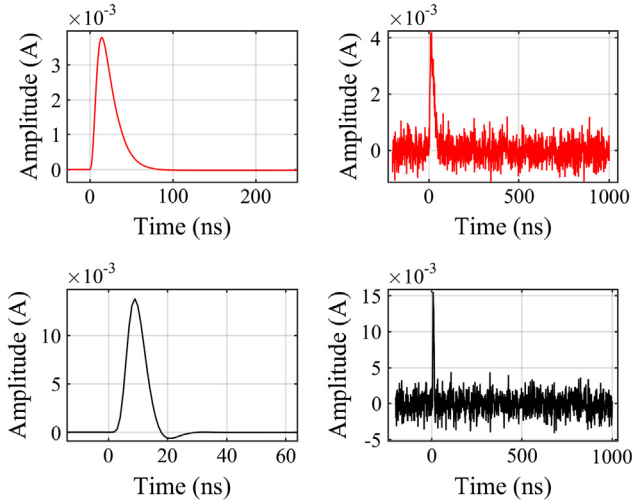

Fig. 2. Filtered pulses according to Eqs. (5) and (6), with and without white noise.

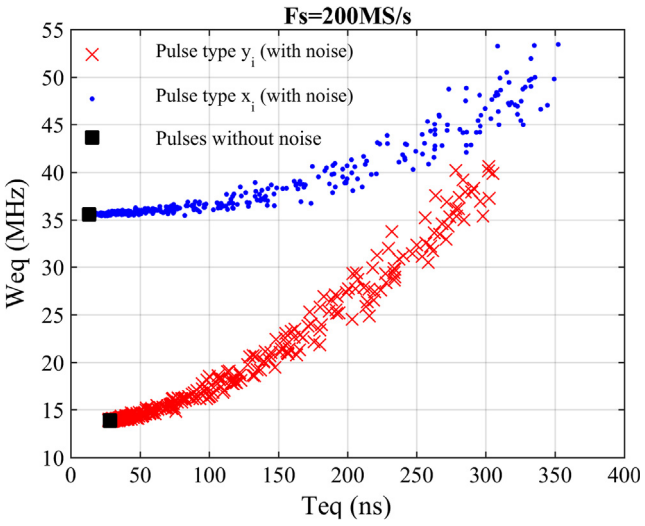

Fig. 3. Classification map for the collection of artificial pulses of type y_i and x_i.

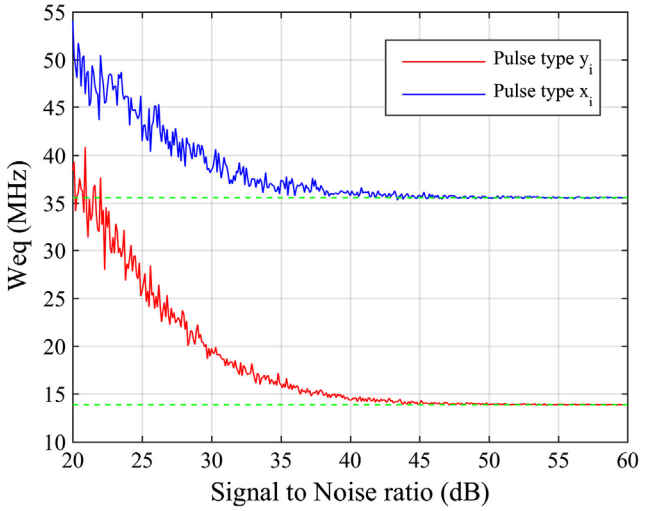

Fig. 4. Change of W_{eq} with signal to noise ratio.

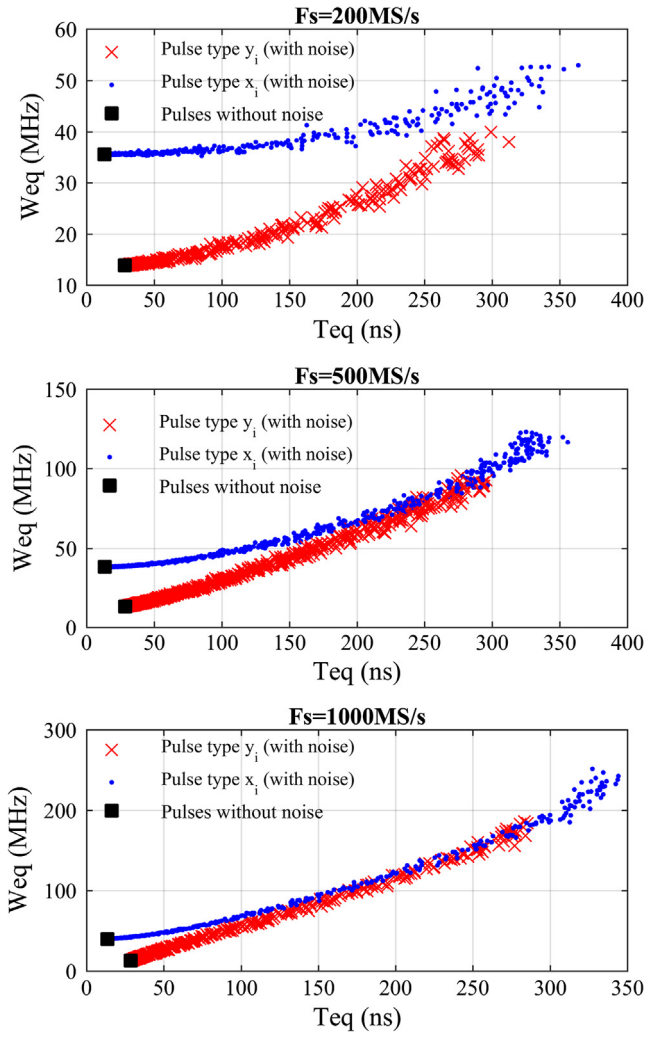

Fig. 5. Classification map for the collection of artificial pulses with varied sampling frequency.

Table 1
Measurements parameters.

Name	VR (mV)	Fs (GS/s)	T (μs)	N (kS)
Test A	0.39	0.2	1	0.2
Test B	0.39	2.5	5	12.5
Test C	0.39	5	2	10
Test D	0.39	1	10	10
Test E	0.39	1	1	1
Test F	0.39	0.2	5	1
Test G	1.56	0.2	5	1

Because of the different shapes, pulses without noise (square dots in Fig. 3) appear as two separated points in the classification map. With the addition of noise, each pulse is represented in such a way that the lower the signal to noise ratio, the higher the values of W_{eq} and T_{eq}. Fig. 4 highlights that the values of W_{eq} increase as the signal to noise ratio decreases, which is also the case for T_{eq}.

Both types of pulses form clearly separated clusters for high values of signal to noise ratio. However there is a trend at lower signal to noise ratios towards the merging of clusters into one single cluster despite pulses being different in shape.

Other interesting result is that the pulses are lying in wide ranges of equivalent time and equivalent bandwidth. This broadening of the cluster might contribute to the overlapping of clusters in the case of multiple PD sources, but also it might be argued that the cluster shape might change due to the signal to noise ratio.

As it was shown in Fig. 3 and Fig. 4, the clusters did not become merged even with a signal to noise ratio of 20 dB, however when the Fs value was varied from 200 MS/s to 1 GS/s, the results of the classification map (Fig. 5) showed that the increase of the Fs had the effect of bringing the clusters together. For the particular case of pulses of the type y_i and x_i studied in this paper, it can be seen that when Fs = 1 GS/s, the effect of noise is so significant that both types of pulses start to form only one cluster.

In practical measurements, since the user is to set the acquisition parameters, not just Fs, being limited by both the specifications of the instrument and by the characteristics of the PD pulses, the signal to noise ratio, unintentionally can be high for some type of pulses but very low for others, particularly being so when multiple PD sources are measured.

The previous theoretical analysis on artificial pulses provided significant results to suggest that the signal to noise ratio has an influence on the classification map. To validate these findings with practical cases, the effect of the acquisition parameters on the

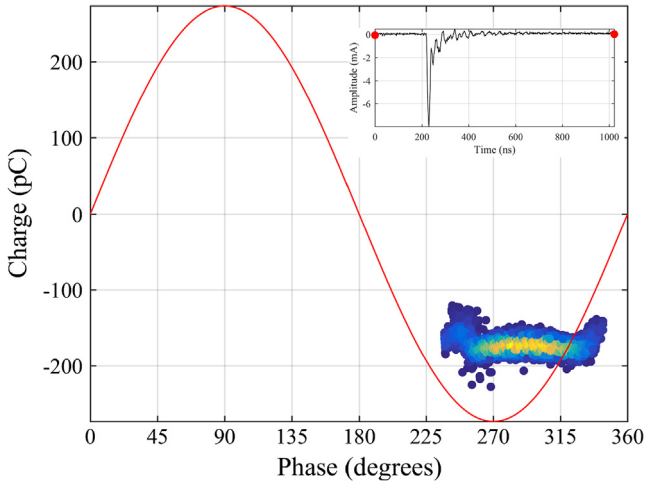

Fig. 6. PRPD pattern for corona discharges and the characteristic waveform of a pulse.

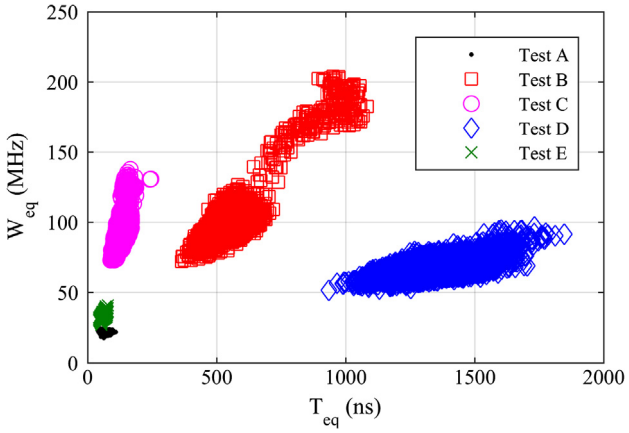

Fig. 7. Classification map $W_{eq} - T_{eq}$ for positive corona.

classification map was investigated in lab measurements, considering single and multiple PD sources.

3.1.2. Classification map for PD pulses

For this analysis, different measurements on a needle-plane electrode were carried out to produce corona discharges. A test voltage of 10 kV was applied to the needle. With this arrangement negative-polarity pulses are produced. However, when positive-polarity pulses were required the needle was connect to ground and the plane to the test voltage, i.e. the connections were reversed.

The self-restoring capability of the insulation (air) and the stability of corona discharges make them suitable as a source of PD pulses having fairly homogeneous shapes and a high repetition rate. Another key factor for choosing this source of PD is that the pulse shape is exponentially damped as was the shape of the artificial simulated pulses. Likewise, the repeatability of the measurements is high so that the experiments can be easily duplicated elsewhere.

The signal to noise ratio was modified for each measurement by setting different acquisition parameters, which are summarized in Table 1. The PRPD pattern shown in Fig. 6 was representative of all measurements in this section which allowed to check for the consistency of the corona discharge source.

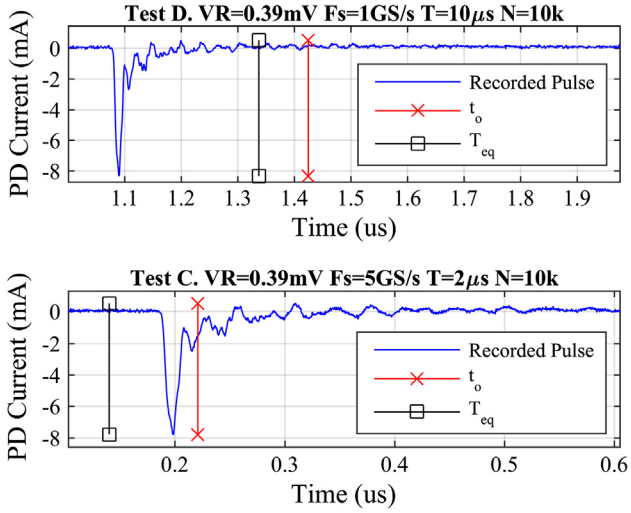

Fig. 8. Effect of the acquisition time T on the results of t_0 and T_{eq} for Test C (top) and Test D (bottom).

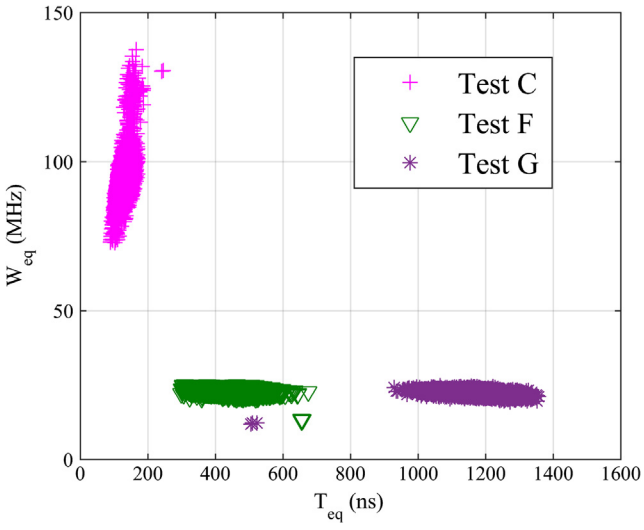

Fig. 9. Classification map $W_{eq} - T_{eq}$ for positive corona, VR variation.

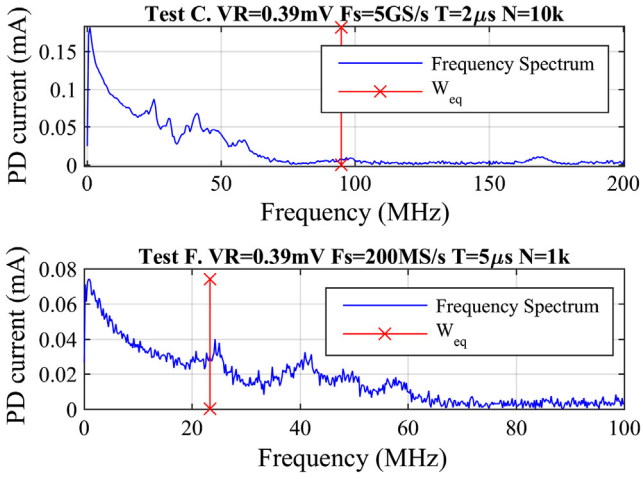

Fig. 10. Effect of the number of samples on the results of W_{eq} for Test C (top) and Test F (bottom).

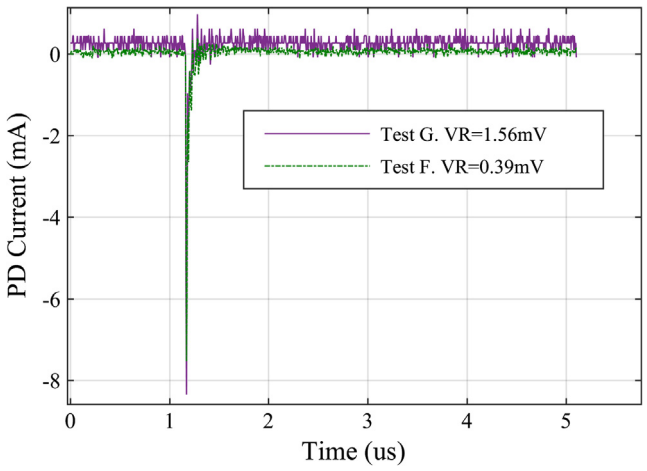

Fig. 11. Corona PD pulses recorded with different vertical scale.

Table 2
Measurements parameters for different PD sources.

Name	PD source	VR (mV)	Fs (GSa/s)	T (μs)	N (kSa)
Test H	Source 1	1.9531	1	2	2
Test I	Source 1	1.9531	0.2	1	0.2
Test J	Source 2	1.9531	0.2	1	0.2
Test K	Source 2	1.9531	1	1	1
Test L	Source 2	1.9531	1	5	5
Test M	Source 2	0.0976	0.2	1	0.2

Source 1 = corona and surface discharges.
Source 2 = corona and free moving particle.

The acquisition parameters in test A to test E led to formation of individual clusters with different magnitudes and shapes in the classification map (Fig. 7) for the same source of corona discharges. The shift of the clusters for test C, B and D towards higher values of T_{eq} was linked to the increase of the acquisition time T, 2 μs, 5 μs and 10 μs while all of them had a comparable number of samples.

The influence of the acquisition time T on T_{eq} is illustrated in Fig. 8, where T_{eq} and t_o are represented for two measured corona pulses from test C and D.

The value of t_0 for a corona pulse with an acquisition time of 2 μs is located closer to the pulse peak, but when the acquisition time is increased to 10 μs the value of t_0 moves to higher values of time, getting away from the pulse peak. Since t_0 is the mean of the time vector weighted by the power of the signal, then it is expected that t_0 moves away from the signal peak as the acquisition time T becomes so long that the signal peak is not predominant anymore; the signal to noise ratio decreases as compared to the signal with shorter acquisition time. It was verified that for all 50,000 pulses recorded in test C, the values of T_{eq} and t_0 were located around the signal peak, but they moved away from the peak in test D as graphically described in Fig. 8.

The comparison between test C and F in Fig. 9 give insights on the increase of W_{eq} with increased number of samples N. The values of W_{eq} for an individual pulse from test C and F are shown in the top row and bottom row respectively in Fig. 10. Pulses recorded with 1k samples and 0.2 GS/s in test F had a W_{eq} within the frequency spectrum of the PD pulse, but when the samples were increased to 10k and 5 GS/s the value of W_{eq} moved towards higher values as in the case of test C. The increase of the number of samples N and sampling frequency leads to a higher frequency resolution in the frequency spectrum (discrete Fourier transform), which means more frequencies contributing to Eq. (3).

Other comparison case comes from test F and G, where the cluster is shifted toward higher values of T_{eq} while the values of W_{eq} almost remained unchanged. It is worth noting that this comparison case is similar to the case in Fig. 5 (Fs = 200 MS/s), where W_{eq} is almost constant for T_{eq} values between roughly 10 to 50 ns.

As can be seen from Table 1, the only difference between tests was a higher vertical resolution for test G that led to a sampling with a lower signal to noise ratio. As an example, Fig. 11 helps to figure out how the pulses from test G are sampled with a lower signal to noise ratio because of the vertical resolution of 1.56 mV, roughly 4 times higher than the vertical resolution of 0.39 mV with which pulses from test F were sampled.

4. Classification map with multiples PD sources

Previous sections already allowed to draw conclusions on how the classification map is affected by varied acquisition parameters. In fact, the case with Fs = 1 GS/s in Fig. 5 proved that pulses with distinct shapes can form clusters that are brought together as a consequence of decreasing signal to noise ratio. The findings from the theoretical study and single PD sources are examined in this section for the case of multiple PD sources.

Laboratory measurements were performed in two distinct combinations of PD sources: corona –surface discharges and corona–free moving particle discharges. Note that according to the convention in Section 3.1.2, the corona source is negative corona, i.e. the

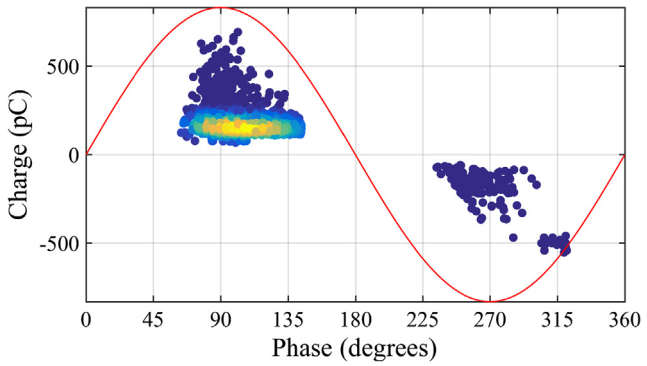

Fig. 12. PRPD pattern for PD Source 1: corona and surface discharges.

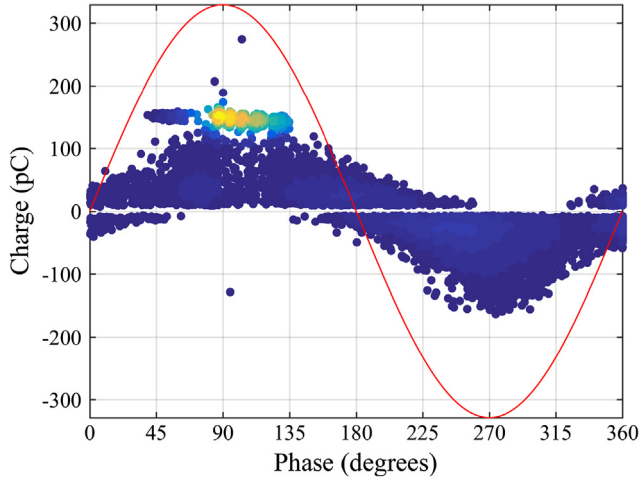

Fig. 13. PRPD pattern for PD Source 2: corona and free moving particle discharges.

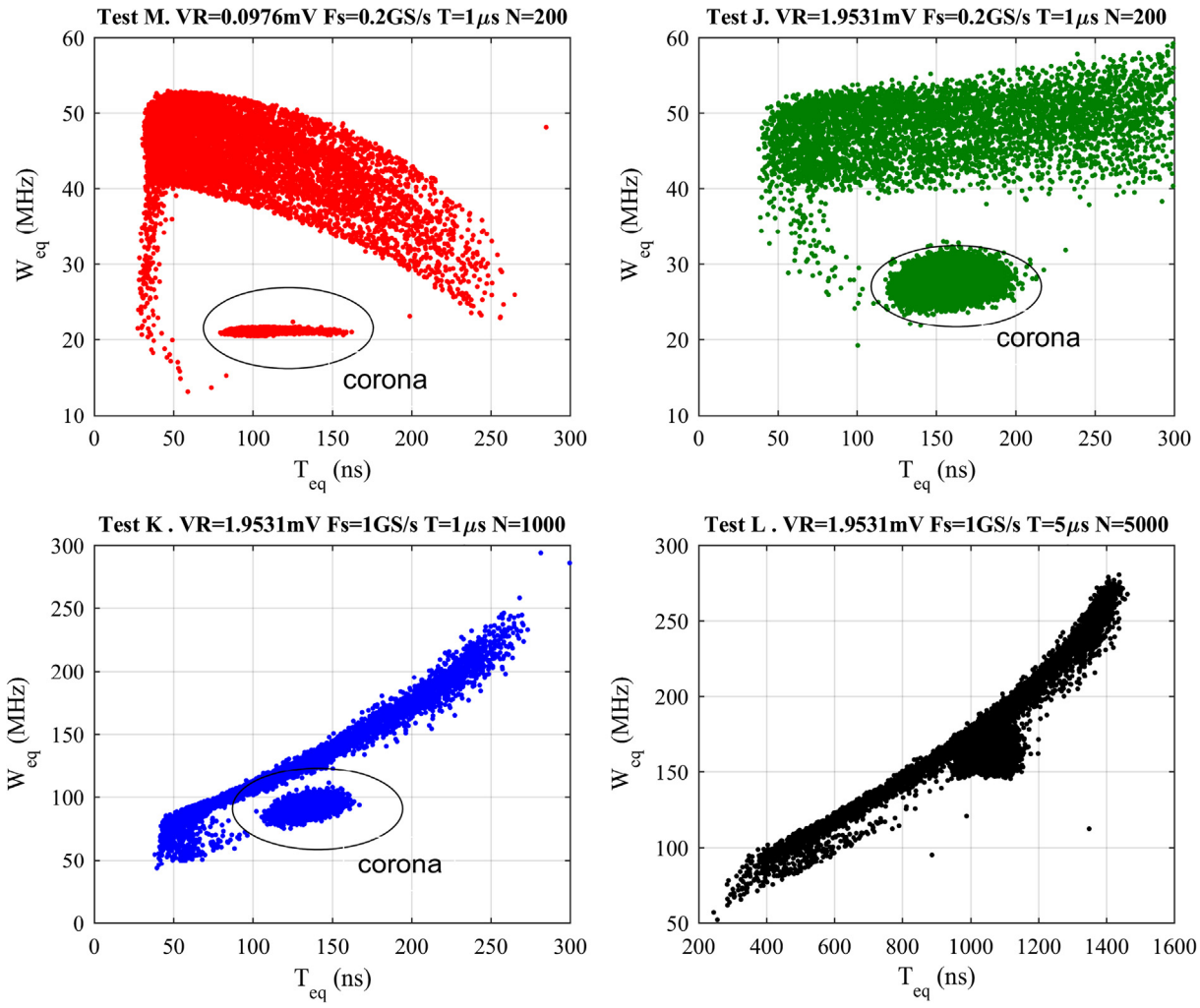

Fig. 14. Classification map for the test cases J, K, L and M (PD Source 2).

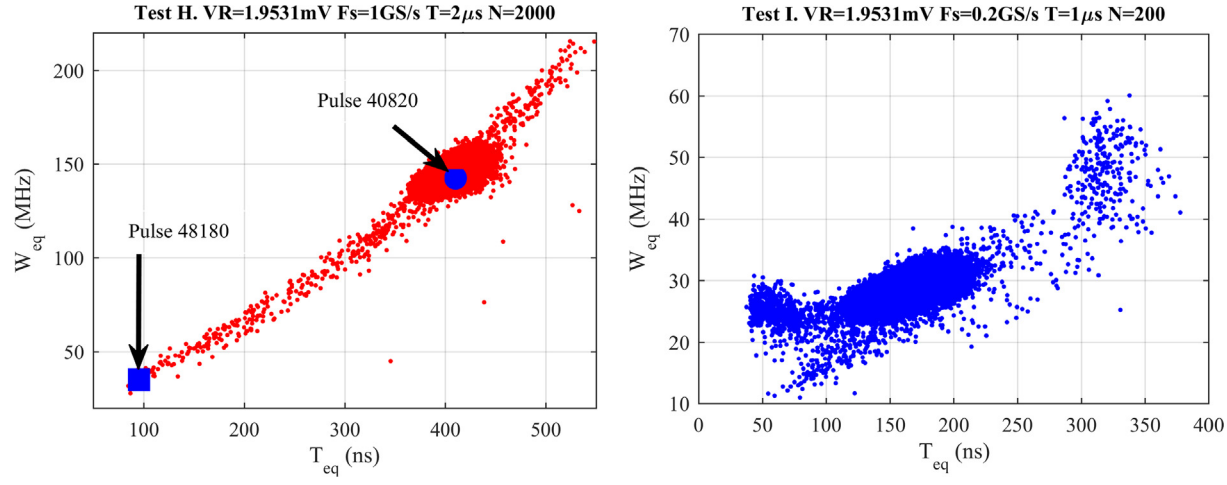

Fig. 15. Classification map for the test cases H and I (PD Source 1).

pulses have positive polarity. In order to set up different signal to noise ratios, the measurements were carried out with different acquisition parameters as depicted in Table 2.

Representative PRPD patterns of both PD source 1 and source 2 are depicted in Figs. 12 and 13.

For the combined PD source 2, corona and free moving particle discharges, the results of the classification map with varied acquisition parameters are shown in Fig. 14.

From test J, K and M, it is possible to distinguish two separated clusters, one corresponding to corona discharges (circled by an

ellipse) and the other one to the discharges from the free moving particle. In test J, the minimum equivalent frequency difference between clusters is 8 MHz, while it is of 10 MHz in test M. This is due to the vertical resolution, that in test M is lower (VR = 0.0976 mV) than in test J (VR = 1.9531 mV), which accounts for a higher signal to noise ratio in test M.

With the decrease of the signal to noise ratio, there is a trend to merge clusters into one single cluster. Particularly, this is the case in test L.

On the other hand, PD source separation by clusters even with a proper selection of acquisition parameters might not always be possible when the shape of the pulses from different sources is very similar. This is illustrated in Fig. 15 where pulses from PD source 1, i.e. combined corona and surface discharges, formed just one single cluster, hindering the separation of sources.

As in cases of previous sections, a lower number of samples as well a short acquisition time tend to result in pulses with a higher signal to noise ratio, which facilitates the separation of PD sources into clusters, e.g. test M. Nevertheless, in test I, pulses from both PD sources formed one single cluster even when the acquisition parameters were varied in a wide range, accordingly to tests in Fig. 15.

After examination of pulses coming from the corona and surface discharges, it turned out that the shapes of the pulses were fairly similar. Two pulses, one from each PD source, were highlighted as an example to recall their pulse shapes. Fig. 16 shows how the pulse shapes are quite homogeneous, being only different in the signal to noise ratio. Conversely, pulse shapes, in any tests from PD source 2, happened to be different as illustrated in Fig. 17.

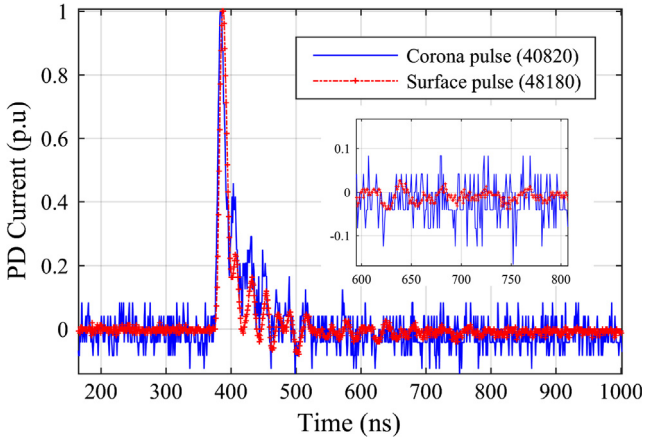

Fig. 16. Comparison of pulse shapes between one corona pulse and one surface pulse.

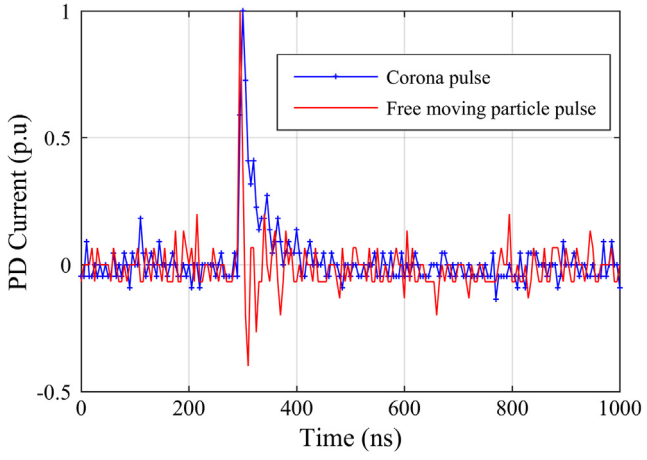

Fig. 17. Comparison of pulse shapes between one corona pulse and one free moving particle pulse.

5. Conclusion

The classification map as intended for recognition of PD sources is based on features (T_{eq} and W_{eq}) that are similar for homogeneous PD pulses, i.e. pulses coming from the same source. However, the laboratory measurements and the theoretical analysis conducted in this paper give insights on how the computation of T_{eq} and W_{eq} are affected by the signal to noise ratio.

When unconventional systems are implemented for the purposes of PD measurements, the signal to noise ratio is in addition affected by the possible combinations of the acquisition parameters, Fs, T, VR and N that the user and the instrument is able to set.

The experiments with single corona discharges led to the conclusion that the variation of Fs, T, VR and N gives rise to clusters with differences in shape and magnitude, even when the PD pulses come from the same source. The values of T_{eq} were shown to increase with longer acquisition times T. Moreover, the increase of the sampling frequency Fs and the number of samples N shifted the values of W_{eq} towards higher values.

In practical measurements of multiple PD sources with unconventional systems, the user sets the vertical resolution, e.g. mV/div scale in the oscilloscope, so that the majority of pulses are displayed in the full screen. Since there will be pulses with higher and smaller amplitudes, then some pulse will be recorded with a high and others with a low signal to noise ratio. A consequence of this is that a collection of PD pulses (even coming from the same source) with a wide range of amplitudes will also have a wide range of values of signal to noise ratio. Since the PD pulses are not homogenous as far as the signal to noise ratio is concerned, Eqs. (2) and (3) lead to a wide range of values of T_{eq} and W_{eq}. This can be seen in Fig. 5, where the cluster spreads over a wide range, increasing the chances for overlapping. The fact that the pulse waveforms, their amplitudes and durations depend on the measuring circuit and on the interaction with the test object makes unfeasible to define a set of acquisition parameters as a guideline for proper unconventional measurements.

The computation of the classification map on pulses from multiple PD sources allowed to separate the sources when the pulse shapes were different and the signal to noise ratio was high enough. Conversely, when the noise became significant, the experimental measurements showed that the clusters for different PD sources tended to merge into one single cluster. This was the case of tests in Fig. 14.

On the other hand, test H and test I proved that when pulse shapes are similar the classification map is unable to separate sources into clusters, regardless of the signal to noise ratio.

Other features of the PD pulses are to be investigated as an attempt to complement and overcome the limitations of the classification map as a tool for separation of PD sources.

References

[1] Yaacob MM, Alsaedi MA, Rashed JR, Dakhil AM, Atyah SF. Review on partial discharge detection techniques related to high voltage power equipment using different sensors. *Photonic Sensors* 2014;4(4):325–37.
[2] High-voltage test techniques-partial discharge measurements. IEC standard 60270; 2000.
[3] Rotating electrical machines–off-line partial discharge measurements on the stator winding insulation of rotating electrical machines. IEC standard 60034-27; 2006.
[4] Gulski E. Computer-aided recognition of partial discharges using statistical tools. Ph.D. dissertation. Delft: EEMCS. TU Delft; 1991.

[5] Zhu M-X, Zhang J-N, Li Y, Wei Y-H, Xue J-Y, Deng J-B, et al. Partial discharge signals separation using cumulative energy function and mathematical morphology gradient. IEEE Trans Dielectr Electr Insul 2016;23(1):482–93.
[6] Alvarez F, Ortego J, Garnacho F, Sanchez-Uran MA. A clustering technique for partial discharge and noise sources identification in power cables by means of waveform parameters. IEEE Trans Dielectr Electr Insul 2016;23(1):469–81.
[7] Granado J, Álvarez-Arroyo C, Torralba A, Rosendo-Macías JA, Chávez J, Burgos-Payán M. Time domain analysis of partial discharges envelope in medium voltage XLPE cables. Electr Power Syst Res 2015;125:220–7.
[8] Albarracin R, Robles G, Martinez-Tarifa JM, Ardila-Rey J. Separation of sources in radiofrequency measurements of partial discharges using time-power ratios maps. ISA Trans 2015;58:389–97.
[9] Robles G, Parrado-Hernández E, Ardila-Rey J, Martínez-Tarifa JM. Multiple partial discharge source discrimination with multiclass support vector machines. Expert Syst Appl 2016;55:417–28.
[10] Ardila-Rey JA, Martinez-Tarifa JM, Robles G. Automatic selection of frequency bands for the power ratios separation technique in partial discharge measurements: Part II, PD source recognition and applications. IEEE Trans Dielectr Electr Insul 2015;22(4):2293–301.
[11] Mor AR, Harmsen DA, Castro Heredia LC. A partial discharge test platform for educational purposes; unpublished.
[12] Mor AR, Morshuis PHF, Smit JJ. Comparison of charge estimation methods in partial discharge cable measurements. IEEE Trans Dielectr Electr Insul 2015;22(2):657–64.
[13] Contin A, Cavallini A, Montanari GC, Pasini G, Puletti F. Digital detection and fuzzy classification of partial discharge signals. IEEE Trans Dielectr Electr Insul 2002;9(3):335–48.
[14] Cavallini A, Contin A, Montanari GC, Puletti F. Advanced PD inference in on-field measurements. I. Noise rejection. IEEE Trans Dielectr Electr Insul 2003;10(2):216–24.
[15] IEEE trial-use guide to the measurement of partial discharges in rotating machinery. IEEE standard 1434; 2000.

Armando Rodrigo Mor is an Industrial Engineer from Universitat Politècnica de València, in Valencia, Spain, with a Ph.D. degree from this university in electrical engineering. During many years he has been working at the High Voltage Laboratory and Plasma Arc Laboratory of the Instituto de Tecnología Eléctrica in Valencia, Spain. Since 2013 he is an Assistant Professor in the Electrical Sustainable Energy Department at Delft University of Technology, in Delft, The Netherlands. His research interests include monitoring and diagnostic, sensors for high voltage applications, high voltage engineering, and HVDC.

Luis Carlos Castro was born in Cali, Colombia in 1986. He received the Bachelor and PhD degree in electrical engineering from Universidad del Valle, Cali, in 2009 and 2015 respectively. Currently, he is a post-doc in the Electrical Sustainable Energy Department at Delft University of Technology, in Delft, The Netherlands. His research interests include accelerated aging of stator insulation, monitoring and diagnostic tests.

Fabio Andrés Muñoz was born in Cali, Colombia, in 1988. He received the B.S. degree in electrical engineering from the Universidad del Valle, Cali, in 2011. He is currently a Ph.D candidate in Electrical Engineering at Universidad del Valle. His main research interests are focused on high voltage engineering, insulation diagnostics and electrical machines.